Short-range order structures of self-assembled Ge quantum dots probed by multiple-scattering extended x-ray absorption fine structure

Zhihu Sun,[1] Shiqiang Wei,[1,*] A. V. Kolobov,[2,†] H. Oyanagi,[3] and K. Brunner[4,‡]

[1]*National Synchrotron Radiation Laboratory, University of Science and Technology of China, Hefei, Anhui 230029, People's Republic of China*

[2]*Laboratory for Advanced Optical Technologies, National Institute of Advanced Industrial Science and Technology, 1-1-1 Higashi, Tsukuba, Ibaraki 305-8562, Japan*

[3]*Photonic Institute, National Institute of Advanced Industrial Science and Technology, 1-1-4 Umezono, Tsukuba, Ibaraki 305-8568, Japan*

[4]*Walter Schottky Institute, Technical University Munich, Am Coulombwall, D-85748 Garching, Germany*

(Received 13 August 2004; published 30 June 2005)

Multiple-scattering extended x-ray absorption fine structure (MS-EXAFS) has been used to investigate the local structures around Ge atoms in self-assembled Ge–Si quantum dots (QDs) grown on Si(001) substrate. The MS effect of Ge QDs is dominated by the scattering path $Ge_0 \rightarrow B_1 \rightarrow B_2 \rightarrow Ge_0$(DS2), which contributes a signal destructively interfering with that of the second shell single-scattering path (SS2). MS-EXAFS analysis reveals that the degree of Ge–Si intermixing for Ge–Si QDs strongly depends on the temperature at which the silicon cap layer is overgrown. It is found that the interatomic distances (R_{Ge-Ge} and R_{Ge-Si}) within the third nearest-neighbor shells in Ge–Si QDs indicate the compressively strained nature of QDs. The present study demonstrates that the MS-EXAFS provides detailed information on the QDs strain and the Ge–Si mixing beyond the nearest neighbors.

DOI: 10.1103/PhysRevB.71.245334 PACS number(s): 61.10.Ht, 68.65.Hb, 81.05.Cy

I. INTRODUCTION

In the last decade, the IV-IV and III-V nanostructures such as quantum dots,[1–5] wires,[6,7] and wells[8,9] have attracted much research interest. Among them the self-assembled Ge/Si quantum dots (QDs) have been a special subject of debate.[2–5] The 4.2% mismatch for the lattice constants between Ge and Si crystals leads to significant strain during the growth of Ge/Si QDs. From the viewpoint of fundamental physics, the strain-driven formation of three-dimensional coherent Ge islands provides a model system for studying the self-assembly of semiconductor nanostructures. The strain can significantly modify the optical and electronic properties of the Ge QDs which have already opened up the route to the development of novel optoelectronics devices[10,11] with relatively simple incorporation into existing Si technology.

Now it is well-known that for the Ge QDs grown on Si in the Stranski-Krastanov (S-K) mode, the intermixing between Ge and Si changes the composition of the grown dots.[2–5,12,13] Therefore the real formation and structure of Ge QDs is much more complicated than that described by the simple S-K mode. Moreover, for the real applications the islands have to be capped with Si to achieve three-dimensional confinement and to avoid oxidation. The capping procedure of the Ge islands is also likely to modify the morphology and structure of Ge QDs. Hence the electronic and optical properties of the Ge islands are strongly affected by their growth conditions.[5,14] In order to deepen the understanding of the growth and capping process of Ge/Si QDs, a simultaneous determination of their strain and composition is of interest. For this purpose, one has to get detailed structural information of Ge QDs. Especially, the short-range structures of the Ge QDs need to be determined.

A routinely used method for the structural studies of the Ge QDs supperlattice is Raman scattering.[15,16] However, in the case of Ge/Si QDs with the thickness of several monolayers (ML), Raman scattering is not very effective, and could not give the local structural information around the Ge atoms directly.[16] This is because of the presence of the two-phonon acoustic peak of the substrate silicon at almost exactly the same frequency as the main peak of germanium, which makes the unambiguous determination of the Ge–Ge peak difficult. An alternative technique for the determination of the local structure of these Ge QDs is extended x-ray absorption fine structure (EXAFS), due to its sensitivity to the short-range order and atomic species surrounding the absorbing atom. We have shown[3,8] that it is easy to obtain the structural information of the first shell for the nanostructure semiconductors by means of EXAFS, e.g., the local structure of $(Ge_4Si_4)_5$ quantum wells[8] and Ge quantum dots[3] were studied with the grazing-incidence fluorescence XAFS. The bond lengths of R_{Ge-Si} (2.38 Å) and R_{Ge-Ge} (2.42 Å) in the first coordination shell of $(Ge_4Si_4)_5$ quantum wells[8] have indicated that the strain is accommodated in the (Ge_4) layers by compressing and bending the Ge–Si and Ge–Ge bonds. A similar result (R_{Ge-Si}=2.37 Å, R_{Ge-Ge}=2.42 Å) has been found for the Si-capped Ge quantum dots self-assembled on Si(001).[3]

Up to date, the XAFS results on the Ge/Si nanostructures are mainly limited to the first shell around Ge atoms.[3,8,12] The elastic strain causes the lattice distortion in the Ge/Si nanostructures which are far different from the highly symmetrical structure of their bulk counterparts. It can be expected that the effect of coherent strain in the higher shell could be determined by the XAFS technique. For accurately calculating the optical and electronic properties of these Ge

and Ge–Si nanostructures, one also needs to reliably determine the tetragonal distortion of the lattice.[17] Therefore a reliable and accurate measurement for the high shells of Ge QDs is essential. However, it is complicated to analyze the EXAFS signals in the high shells owing to the overlap of the contributions from second and third single-scattering (SS) paths, as well as the numerous multiple-scattering (MS) paths. With the developments of the accurate *ab initio* calculations of FEFF[18,19] and GNXAS[20] codes that have considered the multiple-scattering contributions, it is feasible for EXAFS to determine structural information beyond the first coordination shell around specific atoms. There have been some successful works of MS-EXAFS analysis in the recent studies.[21–24] For example, Pascarelli *et al.* have investigated the local structure around As atoms in thin $InAs_xP_{1-x}/InP$ superlattices. Their results have shown that the structural modifications due to tetragonal distortion appear mainly in the second and third shells.[23]

In this work, the MS-EXAFS method is used to study the local structures around Ge atoms in the first three coordination shells for self-assembled Ge QDs capped by Si at different temperatures. The results provide straightforward proof about a different degree of Ge/Si intermixing at different capping temperatures and reveal the strain status of the Ge–Ge bonds within three coordination shells in the Ge QDs. The experimental details and MS-EXAFS analysis are described in Secs. II and III, respectively. First we build up a suitable model for analyzing the diamond structure by performing a detailed MS-EXAFS analysis on Ge crystal. Subsequently this model is simplified and employed to study the local structure of self-assembled Ge QDs grown on Si(001). The obtained results of MS-EXAFS analysis on the Ge QDs are presented in Sec. IV and the discussions about the results are given in Sec. V. Finally a conclusion is summarized in Sec. VI.

II. EXPERIMENT

Two Ge QDs samples were grown by molecular beam epitaxy (MBE) on Si(001) substrates at the same substrate temperature of 510 °C. On a 150 nm Si buffer layer, 7 monolayers (ML) of Ge were deposited at a rate of 0.2 Å/s. The islands are about 20 nm in diameter and 2 nm in height which was shown elsewhere,[3] and have the hut shape and an area density of 1×10^{11} cm^{-2}. One sample was capped by 90 nm Si deposited at the temperature of 510 °C, at a rate linearly increasing from 0.05 to 0.5 Å/s. The other sample was immediately cooled down to 300 °C and a 90-nm Si cap was grown at this temperature. Besides, crystalline Ge (c-Ge) powder and a dilute Ge–Si alloy thin film of $Ge_{0.006}Si_{0.994}$ were used as reference samples.[25]

XAFS measurements for the Ge QDs, c-Ge, and $Ge_{0.006}Si_{0.994}$ alloy were performed at the beamline 13B of Photon Factory, National High Energy Institute of Japan at room temperature. The electron beam energy is 2.5 GeV and the maximum stored current was 400 mA. A 27-pole wiggler with the maximum magnetic field of 1.5 T inserted in the straight section of the storage ring was used. The grazing-incidence fluorescence XAFS[26] was used to collect the data of the Ge QDs and $Ge_{0.006}Si_{0.994}$ alloy, and the transmission XAFS was used for recording the data of c-Ge. For the fluorescence x-ray detection, a 19-element pure Ge solid-state detector[27] was used. The raw data analysis was performed using the NSRL-XAFS3.0 software package[28] according to the standard data analysis procedures. The multiple-scattering data fitting was performed by using FEFFIT of the UWXAFS3.0 software package.[29]

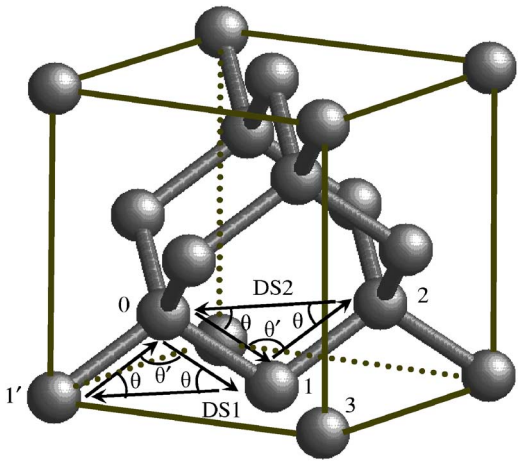

FIG. 1. The diamond structure of crystalline Ge with the representative Ge atom in the first three shells. The number 0 refers to the central absorber Ge atom. Numbers 1 to 3 identify corresponding coordination shells atoms and number 1′ denotes another first coordination shell atom different from atom 1. Two different DS paths DS1 and DS2 are also described.

III. MS-EXAFS ANALYSIS

In this work, all the EXAFS curve-fittings were done in R space. The theoretical scattering amplitude and phase shift functions for all the single-scattering (SS) and MS paths were calculated by using the FEFF7 code,[18,19] starting from the well-known diamond structure of c-Ge. The clusters involving three coordination shells were used for the calculation. By selecting those paths whose amplitude has a weight greater than 3% of the largest one, we obtained 10 pronounced scattering paths. The schematic scattering paths of crystalline Ge are shown in Fig. 1, and the path donations and degeneracies are listed in Table I.

For fitting the EXAFS spectrum of c-Ge, the degeneracy of each path is fixed to the nominal value. In order to decrease the number of independent parameters, the interatomic distances are assumed to relate to changes in the lattice constant due to thermal expansion. The adjustable variable Debye-Waller factor σ^2 for each path is also assumed to be not independent. For example, it is reasonable to assume that the corresponding double scattering (DS) and triple-scattering (TS) paths with the same half path lengths have equal Debye-Waller factors.[21] The muffin-tin potential assumed by FEFF7 is a good approximation for c-Ge due to the electric neutrality of all Ge atoms.[19] Therefore only one

TABLE I. The denotation and degeneracy of paths used in the fits. At the left column, C is the central absorber atom. B_1, B_2, and B_3 identify scattering atoms in the first, second, and third shell, respectively. $B_{1'}$ denote an atom in the first shell different from atom B_1.

Path	Denotation	Degeneracy
$C \rightarrow B_1 \rightarrow C$	SS1	4
$C \rightarrow B_2 \rightarrow C$	SS2	12
$C \rightarrow B_3 \rightarrow C$	SS3	12
$C \rightarrow B_1 \rightarrow B_{1'} \rightarrow C$	DS1	12
$C \rightarrow B_1 \rightarrow B_2 \rightarrow C$	DS2	24
$C \rightarrow B_{1'} \rightarrow B_2 \rightarrow C$	DS3	48
$C \rightarrow B_1 \rightarrow B_3 \rightarrow C$	DS4	48
$C \rightarrow B_2 \rightarrow B_3 \rightarrow C$	DS5	48
$C \rightarrow B_1 \rightarrow C \rightarrow B_1 \rightarrow C$	TS1	4
$C \rightarrow B_1 \rightarrow B_2 \rightarrow B_1 \rightarrow C$	TS2	12

adjustable variable ΔE_0 is needed for all 10 paths. The curve-fitting result is shown in Fig. 2(a) as a dark dashed line and path parameters are listed in Table II.

In general, the radial structural function (RSF) peaks in higher shells may originate from two types of scattering paths. One is SS paths from higher shells, and the other is MS paths. In order to clearly show their contributions to the EXAFS signal of c-Ge, the oscillation curves and amplitude peaks of various scattering paths are shown in Figs. 2(a) and 2(b), respectively. Compared with the SS1, SS2, and SS3 paths, all the other MS paths except DS2 contribute far less to the total oscillation. The oscillation magnitude of DS2 is about 25% as high as that of SS2. Figure 2(b) clearly shows that DS2 is almost out of phase with SS2, therefore the destructive interference between DS2 and SS2 paths strongly damps the intensity of the second peak, as shown clearly in Fig. 2(a).

Since the other MS paths except DS2 contribute very weak signals to the overall EXAFS spectrum of c-Ge, one

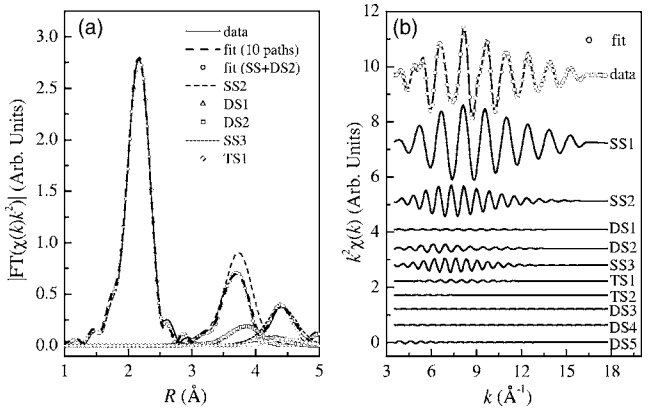

FIG. 2. Contributions of the individual scattering paths to the total EXAFS oscillation function for c-Ge: (a) in R-space, and (b) in k-space. The dark dashed line in Fig. 2(a) shows the fitting result by using all 10 scattering-paths, and empty circles represent the fitting results by using only four paths (SS paths+DS2).

TABLE II. Path parameters obtained from multiple-scattering fit by using all 10 paths for Ge. The parameters in parenthesis are obtained by using only four paths: SS1, SS2, SS3, and DS2. In the fitting procedure, the degeneracies of the paths are fixed.

Path	R(Å)	σ^2 (10^{-3} Å^2)	ΔE_0 (eV)
SS1	2.453±0.005	3.8±0.2	10.1±0.6
	(2.450±0.005)	(3.8±0.2)	(9.8±0.4)
SS2	4.005±0.008	9.8±0.4	10.1±0.6
	(4.001±0.008)	(10.0±0.4)	(9.8±0.4)
SS3	4.696±0.009	12.8±0.8	10.1±0.6
	(4.690±0.009)	(13.5±1.0)	(9.8±0.4)
DS1	4.455±0.009	6.8±1.8	10.1±0.6
DS2	4.455±0.009	6.8±1.8	10.1±0.6
	(4.450±0.009)	(8.0±2.0)	(9.8±0.4)
DS3	5.577±0.012	8.7±5.3	10.1±0.6
DS4	5.577±0.012	8.7±5.3	10.1±0.6
DS5	5.577±0.012	8.7±5.3	10.1±0.6
TS1	4.905±0.010	7.6±0.4	10.1±0.6
TS2	4.905±0.010	7.6±0.4	10.1±0.6

can expect that the experimental data can be well reproduced by considering only the SS paths and DS2. This is indeed the case as shown in Fig. 2(a), where the empty circles represent the fitting result by using only those four paths. Furthermore, in Table II it is obvious that the structural parameters from considering only four paths presented in parenthesis are almost the same as those from considering all 10 scattering paths. The MS-EXAFS analysis on c-Ge suggests that for the diamond structures, only all the SS paths plus DS2 play important roles in determining the structural parameter of the first three shells. Hence only the contributions of all the SS paths and DS2 need to be included in the MS-EXAFS analysis of the Ge QDs.

For the Ge QDs, the MS-EXAFS analysis is much more complicated than that in the case of c-Ge. Since the normal EXAFS result is an average including all the Ge atoms in different surroundings in the Ge QDs, the EXAFS signals coming from the islands and the wetting layer are overlapped. We used a simplified model to separate the EXAFS contributions from the environments around Ge in the islands and the wetting layer. A lot of studies have suggested that Ge islands epitaxially grown on Si(001) substrate form a Ge wetting layer with the equilibrium thickness of about 3 ML at the temperature of 500 °C.[30–32] Therefore we assumed that among the total 7 ML of deposited Ge in the Ge QDs, 3 ML Ge forms a wetting layer and the other 4 ML Ge forms islands. The possible Ge–Si intermixing makes it necessary to include Ge–Ge and Ge–Si pairs in each coordination shell in both the islands and the wetting layer in the EXAFS fits. An average Ge weighting factor x in the islands is assumed as that a percentage $1-x$ of Ge neighbors is replaced by Si atoms due to the Ge–Si intermixing. In order to reduce the number of independent adjustable parameters, the Ge–Ge and Ge–Si coordination numbers of each shell in the islands are related to the total nominal coordination number N, $N_{\mathrm{Ge-Ge}}=Nx$ and $N_{\mathrm{Ge-Si}}=N(1-x)$, respectively. A similar

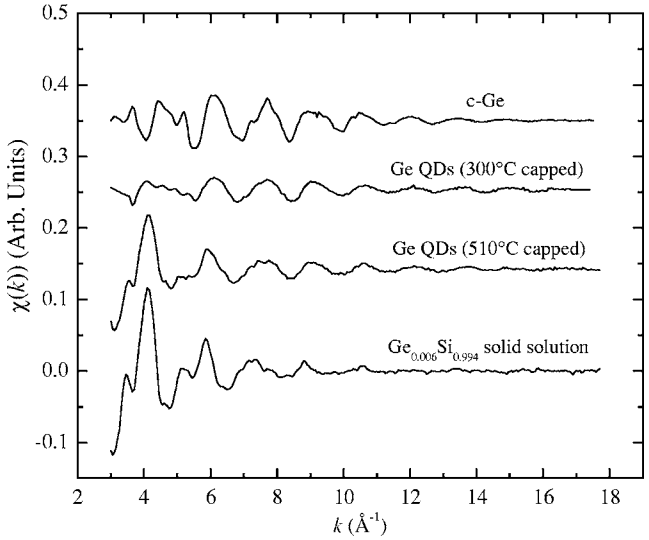

FIG. 3. Ge *K*-edge EXAFS $\chi(k)$ oscillation functions for the Ge QDs samples, c-Ge, and $Ge_{0.006}Si_{0.994}$ dilute solution.

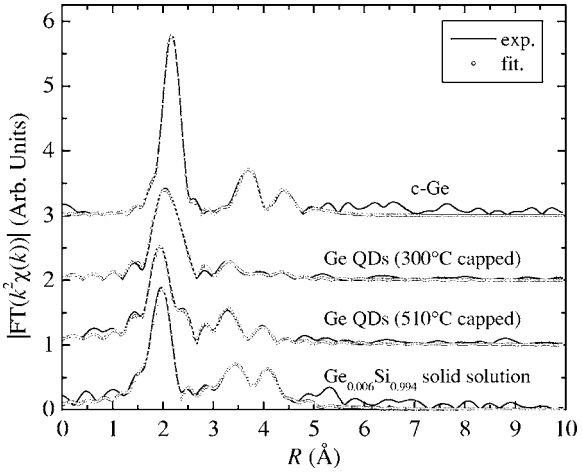

FIG. 4. The radial structural function by Fourier transforming k^2-weighted $\chi(k)$ functions: experiment (solid) and multiple-scattering fit (open circle).

Ge weighting factor y is assigned to the wetting layer. The nearest Ge–Si and Ge–Ge distances in the wetting layer are fixed at 2.38 and 2.42 Å according to these reported values.[8,33,34] The Ge–Ge and Ge–Si interatomic distances of $Ge_{0.5}Si_{0.5}$ alloy in higher shells are used for those in the wetting layer. This consideration is supported by the works of Matsuura *et al.*[33] and Woick *et al.*[34] For the islands, the Ge–Si and Ge–Ge distances in three coordination shells are treated as independent adjustable variables. In each shell a common Debye-Waller factor associated with Ge–Si and Ge–Ge pairs is assigned. The DS2 path is divided into four parts depending on the type of the first- and second-nearest-neighbor atoms: $Ge_0 \rightarrow Ge_1 \rightarrow Ge_2 \rightarrow Ge_0$, $Ge_0 \rightarrow Ge_1 \rightarrow Si_2 \rightarrow Ge_0$, $Ge_0 \rightarrow Si_1 \rightarrow Ge_2 \rightarrow Ge_0$, and $Ge_0 \rightarrow Si_1 \rightarrow Si_2 \rightarrow Ge_0$. The degeneracies of these four paths are also assumed to be related to the above-mentioned Ge weighting factors x and y.

IV. RESULTS

The EXAFS functions $\chi(k)$ of the Ge QDs samples, c-Ge, and $Ge_{0.006}Si_{0.994}$ alloy are shown in Fig. 3. It is easily found that the EXAFS spectra of two Ge QDs samples have remarkably different characteristics, especially in the k range below 8 Å^{-1}. The EXAFS spectrum of the Ge QDs capped by the Si layer at 510 °C shows the highest intensity at $k=4$ Å^{-1}, then it damps very fast with k, which is much different from that of c-Ge possessing a maximum amplitude at 6–8 Å^{-1}, while it is similar to that of $Ge_{0.006}Si_{0.994}$ alloy. This manifests that the Ge atoms are mainly coordinated by the light element Si atoms in the Ge QDs capped by Si at 510 °C. On the contrary, the $\chi(k)$ function of the Ge QDs capped by Si at 300 °C shows a very low intensity at $k<6$ Å^{-1}, which is significantly different from that of the Ge QDs capped by Si at 510 °C.

The obvious differences of the $\chi(k)$ functions for two Ge QDs samples are further exhibited in Fig. 4, where the solid lines show the RSF by Fourier transforming the EXAFS functions $k^2\chi(k)$, and the empty circles display the MS fitting results. The fits were done in the R-intervals including the first three shells, namely, [1.2,4.8] Å, and a typical k-range from 3 to 13 Å^{-1} was used. The RSF curve for c-Ge shows a characteristic feature of the diamond-type tetrahedral structure T_d up to the third nearest neighbor. This feature is essentially identical to that of $Ge_{0.006}Si_{0.994}$ alloy except for a shorter interatomic distance. Compared with c-Ge, the magnitude of the first peak for the 510 °C capped Ge QDs decreases by about 40% with its position shifting toward a smaller distance direction by 0.20 Å. The second- and third-nearest-neighbor peaks are well-resolved for the 510 °C capped Ge QDs. A comparison for the RSFs of 300 and 510 °C capped Ge QDs samples shows that their magnitudes of the first peaks are almost the same, but the peak location of the former is about 0.10 Å larger. In addition, the peaks associated with the high-shell neighbors are much lower for the 300 °C capped Ge QDs. We consider that this is mainly due to the destructive interference between Ge–Ge and Ge–Si pairs as reported by us,[8] Kajiyama *et al.*,[35] and Aldrich *et al.*[36] for the relaxed crystalline $Ge_{0.50}Si_{0.50}$, $Ge_{0.61}Si_{0.39}$, and $Ge_{0.59}Si_{0.41}$ alloys.

The structural parameters of Ge QDs capped at 300 and 510 °C obtained from MS-EXAFS fitting are summarized in Table III. The determination of error bars is consistent with the criteria adopted by the International XAFS Society,[37] i.e., the error bars yielded by FEFFIT are estimated from the square root of the diagonal elements of the correlation matrix. A comparison of the average Ge weighting factors in the islands and the wetting layer indicates that the Ge/Si intermixing prominently occurs in the wetting layer. For the QDs capped at temperatures lower than 360 °C, a lot of studies[4,14,38,39] have suggested that the postgrowth Si capping can hardly change the Ge content in the islands. While for the 510 °C capped Ge QDs strong Ge/Si intermixing takes place between the islands and Si cap.

Here it should be emphasized that Si atoms in the capping layer, besides in the islands, also contribute Si neighbors to Ge in the islands. Therefore the average percentage $1-x$

TABLE III. The structural parameters obtained from multiple-scattering EXAFS fit for the Ge quantum dots. The tabulated interatomic distances (R), Debye-Waller factors (σ^2), and energy shift (ΔE_0) are results of islands. The Si–Si and Ge–Ge interatomic distances in c-Si and c-Ge are also shown for comparison.

Sample	Pair	R(Å)	σ^2 (10^{-3} Å^2)	ΔE_0 (eV)	Ge weighting factor x of islands	Ge weighting factor y of wetting layer
Ge QDs	Ge–Si	2.37±0.01	2.8±0.2	3.1±0.5	0.39±0.10	0.19±0.10
(capped by Si at 510 °C)	Ge–Ge	2.43±0.01	2.8±0.2	5.2±1.2		
	Ge–Si	3.90±0.03	10±2	3.1±0.5		
	Ge–Ge	3.93±0.03	10±2	5.2±1.2		
	Ge–Si	4.58±0.04	15±3	3.1±0.5		
	Ge–Ge	4.61±0.04	15±3	5.2±1.2		
Ge QDs	Ge–Si	2.37±0.01	4.0±0.2	3.5±1.1	0.81±0.10	0.46±0.10
(capped by Si at 300 °C)	Ge–Ge	2.43±0.01	4.0±0.2	4.8±1.1		
	Ge–Si	3.91±0.03	15±2	3.5±1.1		
	Ge–Ge	3.94±0.03	15±2	4.8±1.1		
	Ge–Si	4.58±0.04	19±3	3.5±1.1		
	Ge–Ge	4.62±0.04	19±3	4.8±1.1		
c-Si	Si–Si	2.352				
	Si–Si	3.841				
	Si–Si	4.503				
c-Ge	Ge–Ge	2.447				
	Ge–Ge	3.995				
	Ge–Ge	4.685				

of Si neighbors determined from the EXAFS fits is in fact slightly larger than the real value in the Ge–Si islands, and the real average Ge concentration in the Ge–Si islands is higher than the Ge weighting factor x. For the Ge QDs capped at 300 °C, we estimate that the obtained Ge weighting factor 0.81 is reduced by ~7 % due to the sharp interface effect by using the approach proposed by Soo *et al.*[40] It means that the average Ge concentration in the islands is ~0.9 for the 300 °C capped Ge QDs. For the 510 °C capped Ge QDs, strong Ge/Si intermixing occurs between the islands and the cap, as a result the interface region between the islands and Si cap becomes larger and the average Ge concentration is close to the obtained Ge weighting factor of ~0.4.

Despite the large difference in the composition for the islands capped by Si at 300 and 510 °C, the corresponding Ge–Si and Ge–Ge interatomic distances within three shells are close. The bond lengths $R_{\mathrm{Ge–Si}}$(2.37±0.01 Å) and $R_{\mathrm{Ge–Ge}}$(2.43±0.01 Å)in the islands are almost equal to those in Ge_xSi_{1-x} alloy thin films.[25,33,34] The shortened Ge–Si bond length compared with the sum (2.40 Å) of the covalent radii of Ge and Si, and the contracted nearest Ge–Ge distance relative to the value (2.45 Å) in c-Ge, indicate that the Ge–Si and Ge–Ge bonds in the Ge–Si islands are subject to compressive strain. The most striking result obtained from MS-EXAFS analysis is that the Ge–Ge interatomic distances in the second (3.93±0.03 Å) and third (4.61±0.04 Å) shells are significantly shorter than the corresponding values of 4.00 and 4.69 Å in c-Ge.

V. DISCUSSION

The dependence of the composition of the Ge–Si QDs on the growth temperatures has been extensively investigated by a lot of studies using various methods.[41–49] These include Raman scattering,[41,42] x-ray energy disperse spectrometry,[43] x-ray diffraction[44] and scattering,[45,46] AFM and XPS methods,[47,48] as well as electron energy-loss spectroscopy (EELS).[49] Their results indicate that the Ge concentration in the QD islands gradually increases from ~0.5 to 0.8–1.0 for substrate temperatures decreasing from 700 down to 500 °C. The study in this work reveals that the composition of the Ge QDs is also strongly related to the growth temperatures of Si capping layer. The average Ge concentration in the islands undergoes a drastic increase from ~0.4 to ~0.9 as the Si capping temperature is reduced from 510 to 300 °C. Due to the same growth condition of both Ge QDs, different Si capping temperature is the only factor leading to the obviously different compositions in the islands.

The Ge–Ge interatomic distances obtained by MS-EXAFS allow us to estimate the strain-induced tetragonal distortion of the Ge lattice in the islands. From our EXAFS results the islands grown on Si(001) at 510 °C then capped by Si at 300 °C are prominently composed of pure Ge

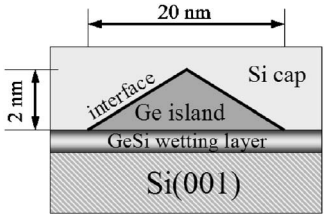

FIG. 5. Schematic cross-sectional geometry of the Ge islands and the Ge wetting layer grown on Si(001).

cluster cores, which is confirmed by the previous etching experiments.[4,50] Due to the coherent epitaxial growth of the islands and the absence of misfit dislocation, the lateral lattice constant $a_{\parallel}$ of the Ge core is approximately equal to that of the wetting layer, which is 5.54 Å according to Vegard's law[51] from the obtained average composition $Ge_{0.46}Si_{0.54}$. Then the average strain parallel to the interface is $\varepsilon_{\parallel}=(a_{\parallel}-a_{Ge})/a_{Ge}=-0.021$ where a_{Ge} is the lattice constant of c-Ge. According to the macroscopic elastic theory,[52] the strain perpendicular ($\varepsilon_{\perp}$) to the interface is related to $\varepsilon_{\parallel}$ by $\varepsilon_{\perp}=(-2C_{11}/C_{12})\varepsilon_{\parallel}=0.016$, where $C_{11}=12.85\times10^{10}$ Pa and $C_{12}=4.83\times10^{10}$ Pa are elastic constants of c-Ge. As the first order approximation, the distortion of Ge–Ge covalent bond due to the biaxial compressive strain can be evaluated from the microscopic model proposed by Woicik *et al.*[34] For the Ge QDs capped at 300 °C, the contraction of the bond length of the Ge–Ge first shell is $\Delta R_1=(2\varepsilon_{\parallel}+\varepsilon_{\perp})R_1/3=-0.021$ Å, and the anisotropical shifts of the tetragonal bond angle are $\Delta\theta=\sqrt{2}(C_{11}+2C_{12})/(C_{11}-C_{12})\Delta R_1/R_1=-2.0°$ and $\Delta\theta'=-\Delta\theta/2=1.0°$, where θ and θ' are the bond angle in- and out-of-plane, respectively. The compression of the Ge–Ge first bond length of 0.021 Å with respect to the value (2.45 Å) in c-Ge is in good agreement with the obtained Ge–Ge bond length (2.43 Å). Calculated from the bond angle shifts, the in-plane Ge–Ge interatomic distance in the second-shell R_2 is 3.92 Å. This value is close to the MS-EXAFS result of 3.93±0.03 Å as shown in Table III. Compared with c-Ge, the Ge–Ge interatomic distances in the second (3.93±0.03 Å) and third (4.61±0.04 Å) shells show a remarkable contraction of 0.07 to 0.08 Å, which indicates that the mismatch strain in the Ge core of the QDs appears mainly in the second and higher Ge–Ge coordination shells.

For the Ge QDs capped by Si at 510 °C, the composition change of islands and wetting layer with respect to the QDs capped at 300 °C shows that strong Si diffusion occurs not only in the surface of the wetting layer but also in the boundary of Ge islands. The average Ge–Ge and Ge–Si coordination numbers in the islands are similar to those of the $Ge_{0.4}Si_{0.6}$ alloy. This indicates that the Ge atoms in the Ge QDs capped at the higher temperature of 510 °C are mostly coordinated by Si neighbors. A schematic model illustrating the cross-sectional geometry of the islands and the wetting layer in Ge QDs is shown in Fig. 5. The size of the Ge islands is 20 nm in diameter and 2 nm in height as shown in our previous AFM image.[3] It indicates that part of the pure Ge phase still remains in the core of Ge islands, since the intermixing length scale is limited to several MLs for the Ge QDs capped at 500 °C.[14] Seen from the EXAFS results in Table III, the Ge–Ge interatomic distances of the second and third shells in the Ge QDs capped at 510 °C are almost the same as those in the Ge QDs capped at 300 °C. Hence the compressive strain in the Ge core of the QDs capped at 510 °C has not been strongly affected by the intermixing Ge–Si layer in the interface region of the islands.

Our MS-EXAFS results have shown that the composition of Ge QDs capped at 300 °C is largely different from that of Ge QDs capped at 510 °C. Only two possible factors can be used to explain the Ge/Si interface intermixing during the Si capping layer growth on Ge dots: one is thermal activation of diffusion, the other is surface segregation (or site exchange). Denker *et al.*[14] have observed different photoluminescence (PL) spectra in two Ge/Si(001) QDs samples grown at 500 °C and capped at different temperatures. For the Ge dots capped at 250 °C and annealed at 500 °C, the island-related PL signal peaks at 0.68 eV, which is quite lower than the PL position (0.80 eV) of the Ge dots capped at 500 °C. Hence the thermal activation of diffusion could not interpret the PL properties of these Ge QDs. On the other hand, in the Si capping process, the Ge/Si intermixing can also be induced by the surface segregation of Ge (or site exchange) due to the large surface mobility of adatoms which allow for decreasing the surface strain as suggested by Oyanagi *et al.*[53] By comparing the segregation energy $E_{seg}\cong0.3$ eV and the activation energy of exchange $E_a\cong1.5$ eV for the Ge/Si(001) quantum structures,[54] we can see that the surface segregation of element Ge is much more sensitive to the capping temperature change than the site exchange. Thus the stronger intermixing of Ge/Si occurs as a result of drastically enhanced surface segregation of Ge atoms as the capping temperature increases from 300 to 510 °C.

VI. CONCLUSION

Grazing-incidence fluorescence XAFS has been used to study the local structures of the self-assembled Ge/Si(001) quantum dots capped by Si at different temperatures. MS-EXAFS analysis was performed to obtain the structural parameters from the first to third coordination shells around Ge atoms for the Ge QDs grown on Si(001). It is unambiguously demonstrated that in the capping process much stronger Ge/Si intermixing occurs at the temperature of 510 °C than at 300 °C. For the Ge dots capped by Si at 300 °C, from the first shell bond lengths R_{Ge-Ge} (2.43 Å) and R_{Ge-Si} (2.37 Å) as well as the estimated bond angle distortion $\Delta\theta(-2.0°)$ and $\Delta\theta'(1.0°)$, the local strain in the nearest neighbor around Ge is mainly accommodated by the bond bending. The observed Ge–Ge interatomic distances of the second (3.93±0.03 Å) and third (4.61±0.04 Å) shells in the islands are 0.07 to 0.08 Å shorter than the corresponding values in c-Ge, indicating the accommodation of compressive strain by stretching the higher shell Ge–Ge bonds. This implies that the mismatch strain in the Ge core of the QDs appears mainly in the second and higher Ge–Ge shells. For Ge dots capped at 510 °C, Ge is strongly intermixed with Si, but the local structure of the compressively strained pure Ge phase in the core of Ge QDs is hardly changed. We consider that the surface segregation of Ge atoms is the prominent cause

for forming $Ge_{0.4}Si_{0.6}$ with a high ratio of Si to Ge at the capping temperature of 510 °C.

ACKNOWLEDGMENTS

This work was supported by National Science Foundation of China (Grant No. 10174068 and 10375059), acknowledge innovation program of Chinese Academy of Sciences, and Specialized Research Fund for the Doctoral Program of Higher Education. Useful discussions of various parts of this work with Professor G. Abstreiter are gratefully acknowledged.

*Corresponding author. Email address: sqwei@ustc.edu.cn
†On leave from A. F. Ioffe Physico-Technical Institute, Am Hubland D-97074urg 194021, Russia.
‡New address: Universität Würzburg, Physikalisches Institut, Am Hubland D-97074 Würzburg, Germany.

[1] J. Stangl, V. Holý, and G. Bauer, Rev. Mod. Phys. **76**, 725 (2004).
[2] K. Brunner, Rep. Prog. Phys. **65**, 27 (2002).
[3] A. V. Kolobov, H. Oyanagi, K. Brunner, P. Schittenhelm, G. Abstreiter, and K. Tanaka, Appl. Phys. Lett. **78**, 451 (2001); A. V. Kolobov, H. Oyanagi, S. Q. Wei, K. Brunner, G. Abstreiter, and K. Tanaka, Phys. Rev. B **66**, 075319 (2002).
[4] M. Stoffel, U. Denker, G. S. Kar, H. Sigg, and O. G. Schmidt, Appl. Phys. Lett. **83**, 2910 (2003).
[5] B. V. Kamenev, L. Tsybeskova, J. M. Baribeau, and D. J. Lockwood, Appl. Phys. Lett. **84**, 1293 (2004).
[6] Y. Hayamizu, M. Yoshita, S. Watanabe, H. Akiyama, L. N. Pfeiffer, and K. W. West, Appl. Phys. Lett. **81**, 4937 (2002).
[7] F. Alsina, P. V. Santos, H. P. Schonherr, R. Notzel, and K. H. Ploog, Phys. Rev. B **67**, 161305 (2002).
[8] S. Q. Wei, H. Oyanagi, K. Sakamoto, Y. Takeda, and T. P. Pearsall, Phys. Rev. B **62**, 1883 (2000).
[9] A. Blom, M. A. Odnoblyudov, I. N. Yassievich, and K. A. Chao, Phys. Rev. B **68**, 165338 (2003).
[10] P. Petroff, A. Lorke, and A. Imamoglu, Phys. Today **54**, 46 (2001).
[11] A. I. Yakimov, A. V. Dvurechenskii, V. V. Kirienko, and A. I. Nikiforov, Appl. Phys. Lett. **80**, 4783 (2002).
[12] F. Boscherini, G. Capellini, L. Di Gaspare, F. Rosei, N. Motta, and S. Mobilio, Appl. Phys. Lett. **76**, 682 (2000).
[13] P. H. Tan, K. Brunner, D. Bougeard, and G. Abstreiter, Phys. Rev. B **68**, 125302 (2003).
[14] U. Denker, M. Stoffel, O. G. Schmidt, and H. Sigg, Appl. Phys. Lett. **82**, 454 (2003).
[15] P. H. Tan, D. Bougeard, G. Abstreiter, and K. Brunner, Appl. Phys. Lett. **84**, 2632 (2004).
[16] A. V. Kolobov, J. Appl. Phys. **87**, 2926 (2000).
[17] K. B. Wong, M. Jaros, I. Morrison, and J. P. Hagon, Phys. Rev. Lett. **60**, 2221 (1988).
[18] J. Mustre de Leon, J. J. Rehr, S. I. Zabinsky, and R. C. Albers, Phys. Rev. B **44**, 4146 (1991).
[19] J. J. Rehr and R. C. Albers, Rev. Mod. Phys. **72**, 621 (2000).
[20] A. Filipponi, A. Di Cicco, and C. R. Natoli, Phys. Rev. B **52**, 15122 (1995).
[21] A. I. Frenkel, E. A. Stern, M. Qian, and M. Newville, Phys. Rev. B **48**, 12449 (1993).
[22] A. Filipponi and A. Di Cicco, Phys. Rev. B **52**, 15135 (1995).
[23] S. Pascarelli, F. Boscherini, C. Lamberti, and S. Mobilio, Phys. Rev. B **56**, 1936 (1997).
[24] V. Simoneta, Y. Calzavara, J. L. Hazemann, R. Argoud, O. Geaymond, and D. Raoux, J. Chem. Phys. **116**, 2997 (2002).
[25] S. Q. Wei, H. Oyanagi, H. Kawanami, K. Sakamoto, T. Sakamoto, K. Tamura, N. L. Saini, and K. Uosaki, J. Appl. Phys. **82**, 4810 (1997).
[26] H. Oyanagi, R. Shioda, Y. Kuwahara, and K. Haga, J. Synchrotron Radiat. **2**, 99 (1995).
[27] H. Oyanagi, M. Martini, and M. Saito, Nucl. Instrum. Methods Phys. Res. A **403**, 58 (1998).
[28] W. J. Zhong and S. Q. Wei, J. Chin. Univ. Sci. Technol. **31**, 328 (2001).
[29] E. A. Stern, M. Newville, B. Ravel, Y. Yakoby, and D. Haskel, Physica B **208&209**, 117 (1995).
[30] Y. M. Mo, D. E. Savage, B. S. Swartzentruber, and M. G. Lagally, Phys. Rev. Lett. **65**, 1020 (1990).
[31] Y. Zhang and J. Drucker, J. Appl. Phys. **93**, 9583 (2003).
[32] M. A. Makeev, W. Yu, and A. Madhukar, Phys. Rev. B **68**, 195301 (2003).
[33] M. Matsuura, J. M. Tonnerre, and G. S. Cargill, III, Phys. Rev. B **44**, 3842 (1991).
[34] J. C. Woicik, C. E. Bouldin, K. E. Miyano, and C. A. King, Phys. Rev. B **55**, 15386 (1997).
[35] H. Kajiyama, S. Muramatsu, T. Shimada, and Y. Nishino, Phys. Rev. B **45**, 14005 (1992).
[36] D. B. Aldrich, R. J. Nemanich, and D. E. Sayers, Phys. Rev. B **50**, 15026 (1994).
[37] F. W. Lytle, D. E. Sayers, and E. A. Stern, Physica B **158**, 701 (1989).
[38] A. Rastelli, E. Mueller, and H. von Kaenel, Appl. Phys. Lett. **80**, 1438 (2002).
[39] J. Stangl, A. Hesse, V. Holý, Z. Zhong, G. Bauer, U. Denker, and O. G. Schmidt, Appl. Phys. Lett. **82**, 2251 (2003).
[40] Y. L. Soo, G. Kioseoglou, S. Huang, S. Kim, Y. H. Kao, Y. H. Peng, and H. H. Cheng, Appl. Phys. Lett. **78**, 3684 (2001).
[41] X. Wang, Z. Jiang, H. Zhu, F. Lu, D. Huang, X. Liu, C. Hu, Y. Chen, Z. Zhu, and T. Yao, Appl. Phys. Lett. **71**, 3543 (1997).
[42] J. Zhu, C. Miesner, K. Brunner, and G. Abstreiter, Appl. Phys. Lett. **75**, 2395 (1999).
[43] S. A. Chaparro, J. Drucker, Y. Zhang, D. Chandrasekhar, M. R. McCartney, and D. J. Smith, Phys. Rev. Lett. **83**, 1199 (1999).
[44] Z. M. Jiang, X. M. Jiang, W. R. Jiang, Q. J. Jia, W. L. Zheng, and D. C. Qian, Appl. Phys. Lett. **76**, 3397 (2000).
[45] R. Magalhaes-Paniago, G. Medeiros-Ribeiro, A. Malachias, S. Kycia, T. I. Kamins, and R. Stan Williams, Phys. Rev. B **66**, 245312 (2002).
[46] A. Hesse, J. Stangl, V. Holy, T. Roch, and G. Bauer, Phys. Rev. B **66**, 085321 (2002).
[47] G. Capellini, M. De Seta, and F. Evangelisti, Appl. Phys. Lett. **78**, 303 (2001).

[48] M. De Seta, G. Capellini, F. Evangelisti, and S. Spinella, J. Appl. Phys. **92**, 614 (2002).
[49] M. Floyd, Y. Zhang, K. P. Driver, J. Drucker, P. A. Crozier, and D. J. Smith, Appl. Phys. Lett. **82**, 1473 (2003).
[50] O. G. Schmidt, U. Denker, S. Christiansen, and F. Ernst, Appl. Phys. Lett. **81**, 2614 (2002).
[51] J. C. Mikkenlsen and J. B. Boyce, Phys. Rev. Lett. **49**, 1412 (1982).
[52] J. Hornstra and W. J. Bartels, J. Cryst. Growth **44**, 513 (1978).
[53] H. Oyanagi, K. Sakamoto, R. Shioda, and T. Sakamoto, Jpn. J. Appl. Phys., Part 1 **33**, 3545 (1994).
[54] P. Boguslawski and J. Bernholc, Phys. Rev. Lett. **88**, 166101 (2002).